Feedback-induced bistability of an optically levitated nanoparticle: A Fokker-Planck treatment

Wenchao Ge, Brandon Rodenburg, and M. Bhattacharya

Phys. Rev. A **94**, 023808 — Published 1 August 2016

DOI: 10.1103/PhysRevA.94.023808

Feedback-induced Bistability of an Optically Levitated Nanoparticle: A Fokker-Planck Treatment

Wenchao Ge, Brandon Rodenburg, and M. Bhattacharya
School of Physics and Astronomy, Rochester Institute of Technology, 84 Lomb Memorial Drive, Rochester, NY 14623, USA
(Dated: July 20, 2016)

Optically levitated nanoparticles have recently emerged as versatile platforms for investigating macroscopic quantum mechanics and enabling ultrasensitive metrology. In this article we theoretically consider two damping regimes of an optically levitated nanoparticle cooled by cavityless parametric feedback. Our treatment is based on a generalized Fokker-Planck equation derived from the quantum master equation presented recently and shown to agree very well with experiment [1]. For low damping, we find that the resulting Wigner function yields the single-peaked oscillator position distribution and recovers the appropriate energy distribution derived earlier using a classical theory and verified experimentally [2]. For high damping, in contrast, we predict a double-peaked position distribution, which we trace to an underlying bistability induced by feedback. Unlike in cavity-based optomechanics, stochastic processes play a major role in determining the bistable behavior. To support our conclusions, we present analytical expressions as well as numerical simulations using the truncated Wigner function approach. Our work opens up the prospect of developing bistability-based devices, characterization of phase-space dynamics, and investigation of the quantum-classical transition using levitated nanoparticles.

PACS numbers: 42.50.Wk, 62.25.-g, 05.10.Gg

I. INTRODUCTION

Optical levitation of small particles was first demonstrated by Ashkin in seminal work performed more than four decades ago [3]. Since then, optical trapping has become a powerful tool for manipulating atoms [4], dielectric particles [5], and biological systems [6]. Recently, optically levitated dielectric microscopic [7–9] and nanoscopic [2, 10–13] particles have been cooled in both cavity-based [14, 15] and cavity-free [16] setups, paving the way for macroscopic quantum mechanics [17–21] and ultrasensitive metrology [22–25]. Parallel to ongoing experiments aimed at preparing the nanoparticle ground state in a cavityless configuration, a quantum model of parametric feedback cooling of an optically levitated nanoparticle was presented recently [1]. This model provided a master equation, whose predictions regarding feedback cooling agreed very well with experimental data in the classical regime.

In this article, we derive a Fokker-Planck (FP) equation from the above-mentioned master equation. As is well known, the FP equation is well-suited for analysing the phase-space distribution for a quantum system, is convenient for studying the quantum-classical boundary, and is also an efficient calculational tool for dealing with high excitation numbers which make simulation of the master equation computationally difficult [26]. In the present work, we use the FP approach to analyse one of the features which strongly distinguishes parametric feedback cooling from other active feedback schemes for optomechanical cooling [27–31], namely the highly nonlinear nature of the resultant damping. It was shown theoretically as well as experimentally earlier that such damping generally results in nonlinear phonon dynamics for - and specifically nonexponential loss of energy from - the nanoparticle [1]. Such behavior stands in contrast to most optomechanical systems where the mechanical element can be described as a linearly damped oscillator even when coupled to optical radiation, and linear response theory yields a satisfactory description [20].

We examine two qualitatively different regimes of nanoparticle feedback damping, namely low and high damping, respectively. In the low damping regime, we obtain a Wigner function which yields a single-peaked position distribution as well as the energy distribution calculated earlier using a classical theory and verified experimentally [2, 10]. In the high damping regime, in contrast, we predict a *double-peaked* position distribution which we trace to an underlying parametric feedback-induced bistability. Unlike in cavity-based systems, where bistability can be explained using the mean (drift-like) effects of active [27–31] or passive [32–36] feedback, in our case the diffusive processes present in the system provide a major contribution to bistable behavior [37]. Our results open the way to the investigation of levitated cavity-free optomechanical systems in relation to bistability-related fundamental effects such as squeezing [38] and entanglement [39], and for the construction of useful devices [40].

The remainder of this paper is arranged as follows. Section II introduces the FP equation and recovers analytically the predictions of the master equation regarding the nanoparticle phonon number. Section III introduces the truncated Wigner distribution and reproduces numerically the results of the master equation, showing the validity of the truncation. Further, it describes analytically and numerically the low and high damping regimes, respectively, for the levitated nanoparticle. Section IV supplies a conclusion.

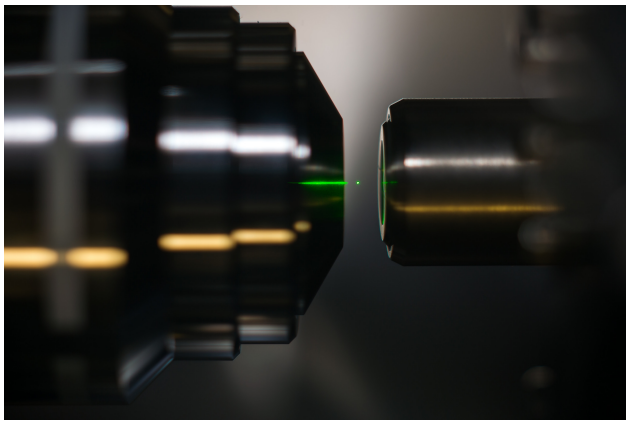

FIG. 1. Levitated nanoparticle considered in this article. Photograph courtesy of A. N. Vamivakas and J. Adam Fenster, University of Rochester.

II. THE FP EQUATION

The system under consideration is a dielectric nanoparticle trapped at the focus of a single Gaussian beam as described in earlier work [1, 10, 13, 16], and shown in Fig. 1. The motion of the trapped nanoparticle is detected by an additional probe beam. The detected signal is phase-shifted, frequency doubled, and then fed back to the trap beam to cool its motion. For small oscillation amplitudes, motion along each trap direction can be treated separately [12]. The master equation for the nanoparticle z-motion is given by [1]

$$\begin{aligned}\dot{\rho} =& -i[\omega_z b_z^\dagger b_z, \rho] - \left(\frac{A_t + A_p + D_p}{2}\right)\mathcal{D}[Q_z]\rho \\ &- \frac{D_q}{2}\mathcal{D}[P_z]\rho - i\frac{\gamma_g}{2}[Q_z, \{P_z, \rho\}] \\ &- i\gamma_f\left[Q_z^3, \{P_z, \rho\}\right] - \Gamma_f\mathcal{D}[Q_z^3]\rho, \end{aligned} \tag{1}$$

where ρ is the nanoparticle density matrix. The first term on the right hand side of the above equation represents the harmonic oscillation with trapping frequency ω_z. The second and third terms arise from the diffusion of the nanoparticle momentum and position, respectively, where $A_t(A_p)$ is the scattering due to the trap (probe) field, and $D_p = 2\gamma_g N_0$ and $D_q = \gamma_g/(6N_0)$ are the coefficients of momentum and the position diffusion, respectively, due to the background gas [41]. $N_0 = k_B T/\hbar\omega_z \gg 1$ is the thermal phonon number with k_B the Boltzmann constant and T the gas temperature. The fourth term describes the damping due to the gas at the rate $\gamma_g = \eta_f/2m$, where η_f is the friction force per unit volume due to the gas and m is the mass of the nanoparticle. The fifth term and the sixth terms correspond to the nonlinear (in oscillator variables) feedback damping and the corresponding feedback backaction, respectively. The feedback drift and diffusion are characterized by the coefficients $\gamma_f = \chi^2\Phi G$, and $\Gamma_f = \chi^2\Phi G^2$, respectively, where χ is the scaled optomechanical coupling, Φ is the average detected flux of the probe photons, and G is the feedback gain. The annihilation (creation) operator of the nanoparticle motion along z direction is b_z ($b_z^\dagger$). The dimensionless position and momentum operators are $Q_z = b_z^\dagger + b_z$ and $P_z = i(b^\dagger - b)$, respectively. The Lindblad superoperator in Eq. (1) is $\mathcal{D}[Q_z]\rho = Q_z^\dagger Q_z\rho + \rho Q_z^\dagger Q_z - 2Q_z\rho Q_z^\dagger$.

The Wigner function for a quantum system with the density matrix ρ is defined as [42]

$$W(X,P) = \frac{1}{\pi\hbar}\int e^{\frac{P\xi}{i\hbar}}\langle X + \xi/2|\,\rho\,|X - \xi/2\rangle\, d\xi, \tag{2}$$

where $|X\rangle$ is the eigenstate of the system at the position X. For the dimensionless position operator Q_z, we have $Q_z|X\rangle = \sqrt{2}\frac{X}{x_0}|X\rangle$. For the dimensionless momentum operator P_z, we have $P_z|X\rangle = \sqrt{2}\frac{i\hbar}{p_0}\frac{\partial}{\partial X}|X\rangle$. Here $x_0 = \sqrt{\frac{\hbar}{m\omega_z}}$ and $p_0 = \sqrt{\hbar m\omega_z}$. By applying the position states $\langle X + \xi/2|$ and $|X - \xi/2\rangle$ from left and right to Eq. (1) and performing the integration, we obtain the FP equation for the Wigner distribution as

$$\begin{aligned}\frac{\partial W(x,p,t)}{\partial t} =& \left(-\omega_z p\frac{\partial}{\partial x} + \omega_z x\frac{\partial}{\partial p}\right)W(x,p,t) + \left[2\gamma_g\frac{\partial}{\partial p}p + (A_t + A_p + D_p)\frac{\partial^2}{\partial p^2} + D_q\frac{\partial^2}{\partial x^2}\right]W(x,p,t) \\ &+ \left(24\gamma_f x^2\frac{\partial}{\partial p}p - 2\gamma_f\frac{\partial^3}{\partial p^3}p\right)W(x,p,t) + \left(72\Gamma_f x^4\frac{\partial^2}{\partial p^2} - 12\Gamma_f x^2\frac{\partial^4}{\partial p^4} + \frac{\Gamma_f}{2}\frac{\partial^6}{\partial p^6}\right)W(x,p,t), \end{aligned} \tag{3}$$

where we have defined the dimensionless position and momentum $x = X/x_0$ and $p = P/p_0$, respectively. The first term on the right-hand-side of Eq. (3) represents the mechanical oscillation, the second term includes the gas damping, the gas diffusion and the scattering from optical fields, respectively, the third term originates from the nonlinear feedback damping, and the fourth term accounts for the diffusion due to feedback backaction. Since Eq. (3) is a complicated sixth order partial differential equation, we begin below by first considering some simple limits before moving on to more complex situations.

A. No feedback

We first consider the case when there is no feedback applied to the optically trapped nanoparticle. In this case, we can set the feedback gain $G = 0$, such that $\gamma_f = \Gamma_f = 0$. Written in a compact form, the FP equation for the Wigner function is then given by

$$\frac{\partial W}{\partial t} = \gamma_{ij}\frac{\partial}{\partial x_i}(x_j W) + D_{ij}\frac{\partial^2 W}{\partial x_i \partial x_j}, \tag{4}$$

where $x_1 = x$, $x_2 = p$, and the drift matrix γ and the diffusion matrix are given by

$$\gamma = \begin{pmatrix} 0 & -\omega_z \\ \omega_z & 2\gamma_g \end{pmatrix}, \tag{5}$$

and

$$D = \begin{pmatrix} D_q & 0 \\ 0 & A_t + A_p + D_p \end{pmatrix}, \tag{6}$$

respectively. It can be readily seen by inspection that D is positive definite, i.e. that it is symmetric and its eigenvalues are positive.

For any initial condition, the system reaches a steady-state after a long enough time and then $\partial W/\partial t = 0$. We consider an ansatz of the steady-state solution to the W function as a Gaussian distribution [43], i.e.

$$W_{\rm ss}(x,p) = \frac{1}{2\pi}\frac{1}{\sqrt{ab-c^2}} e^{-\frac{1}{2(ab-c^2)}(bx^2 + ap^2 - 2cxp)}. \tag{7}$$

By substituting the expression of $W_{\rm ss}(x,p)$ into Eq. (4), we obtain the a, b, c as

$$a = \frac{A_t + A_p + D_p + D_q}{2\gamma_g} + \frac{2\gamma_g D_q}{\omega_z^2}, \tag{8}$$

$$b = \frac{A_t + A_p + D_p + D_q}{2\gamma_g}, \tag{9}$$

$$c = -\frac{D_q}{\omega_z}. \tag{10}$$

From the Wigner function, we obtain the steady-state moments of the nanoparticle as

$$\langle x^2\rangle_{\rm ss} = \frac{A_t + A_p + D_p + D_q}{2\gamma_g} + \frac{2\gamma_g D_q}{\omega_z^2}, \tag{11}$$

$$\langle p^2\rangle_{\rm ss} = \frac{A_t + A_p + D_p + D_q}{2\gamma_g}, \tag{12}$$

$$\langle xp\rangle_{\rm ss} = -\frac{D_q}{\omega_z} \tag{13}$$

If $(\gamma_g, D_q) \ll \omega_z$, which applies experimentally, equipartition is exact and $\langle x^2\rangle_{\rm ss} = \langle p^2\rangle_{\rm ss}$. The mean steady-state phonon number of the nanoparticle without feedback cooling is given by [42]

$$\begin{aligned}\langle n\rangle_{\rm ss} &= \int W_{\rm ss}\left(\frac{x^2+p^2}{2}\right)dxdp - \frac{1}{2} \\ &= \frac{\langle x^2\rangle_{\rm ss}}{2} + \frac{\langle p^2\rangle_{\rm ss}}{2} - \frac{1}{2} \\ &= \frac{A_t + A_p + D_p + D_q}{2\gamma_g} + \frac{\gamma_g}{\omega_z^2}D_q - \frac{1}{2},\end{aligned} \tag{14}$$

where $n = b_z^\dagger b_z$. This result shows the thermal equilibrium of the particle with its surrounding gas in the presence of the trapping and probing lasers. We note that in this regime the nanoparticle is linearly damped by the gas. For high gas pressure and high temperature, Eq. (14) implies $\langle n\rangle_{\rm ss} \approx D_p/(2\gamma_g) = k_B T/(\hbar\omega_z)$.

B. With parametric feedback

We now consider the case where the feedback is turned on, which cools the nanoparticle into a lower mean phonon number state. In this case we were unable to solve for the Wigner function analytically. Instead, we employed the full FP equation in Eq. (3) to generate phase-space moments of the nanoparticle. We multiplied system variables with Eq. (3) and integrated over phase-space to obtain the following relevant equations

$$\langle \dot{x^2}\rangle = 2\omega_z\langle xp\rangle + 2D_q, \tag{15}$$

$$\begin{aligned}\langle \dot{p^2}\rangle = &-2\omega_z\langle xp\rangle - 4\gamma_g\langle p^2\rangle + 2(A_t + A_p + D_p) \\ &+144\Gamma_f\langle x^4\rangle - 48\gamma_f\langle x^2p^2\rangle,\end{aligned} \tag{16}$$

$$\begin{aligned}\langle \dot{xp}\rangle = &\omega_z\langle p^2\rangle - \omega_z\langle x^2\rangle - 2\gamma_g\langle xp\rangle \\ &-24\gamma_f\langle x^3p\rangle,\end{aligned} \tag{17}$$

$$\begin{aligned}\langle \dot{x^3p}\rangle = &3\omega_z\langle x^2p^2\rangle - \omega_z\langle x^4\rangle - 2\gamma_g\langle x^3p\rangle \\ &-24\gamma_f\langle x^5p\rangle,\end{aligned} \tag{18}$$

$$\langle \dot{x^4}\rangle = 4\omega_z\langle x^3p\rangle + 12D_q\langle x^2\rangle, \tag{19}$$

$$\langle \dot{x^6}\rangle = 6\omega_z\langle x^5p\rangle + 30D_q\langle x^4\rangle, \tag{20}$$

where for any moment $f(x,p)$, $\langle f(x,p)\rangle = \int W(x,p,t)f(x,p)dxdp$ and we have used the boundary conditions $\frac{\partial^j W(x,p,t)}{\partial^j x}|_{x=\pm\infty} = 0$ $(j = 0,1)$, and $\frac{\partial^k W(x,p,t)}{\partial p^k}|_{p=\pm\infty} = 0$ $(k = 0,\ldots,5)$ [44]. Equations (15)–(20) are not a closed set of equations for all involved moments, but as we will see below, they contain all the information required for solving for the steady state phonon number. In the steady-state, we obtain

$$\langle p^2\rangle_{\rm ss} = \left(1 - 72\frac{\gamma_f D_q}{\omega_z^2}\right)\langle x^2\rangle_{\rm ss} - \frac{2\gamma_g D_q}{\omega_z^2}, \tag{21}$$

$$A\langle x^4\rangle_{\rm ss} + B\langle x^2\rangle_{\rm ss} + C = 0, \tag{22}$$

with the coefficients $A = 8\gamma_f\left(1 - 9\frac{\Gamma_f}{\gamma_f} - 120\frac{\gamma_f D_q}{\omega_z^2}\right)$, $B = 2\gamma_g\left(1 - 96\frac{\gamma_f D_q}{\omega_z^2}\right)$, and $C = A_t + A_p + D_p + D_q + \frac{4\gamma_g^2 D_q}{\omega_z^2}$. Comparing Eq. (21) with Eqs. (11) and (12) we see that there is an additional deviation from exact equipartition due to the parametric feedback. For typical experimental parameters, $\gamma_f \ll \omega_z$, and this deviation is quite small.

In order to solve Eq. (22), we further assume that the position is described approximately by a zero-mean Gaussian distribution (as for a thermal state), which gives the relation $\langle x^4\rangle = 3\langle x^2\rangle^2$. After some rearrangement Eq. (22) can be rewritten as

$$2J\langle x^2\rangle_{\rm ss}^2 + 2\gamma_g\langle x^2\rangle_{\rm ss} - (A_t + A_p + D_p) = 0, \tag{23}$$

where $J = 12(\gamma_f - 9\Gamma_f)$ and we have neglected all the terms proportional to D_q since $D_q \ll \omega_z$ in the experiment. We obtain from Eq. (23) the steady-state position-squared mean as

$$\langle x^2\rangle_{\rm ss} = -\frac{\gamma_g}{2J} + \frac{\sqrt{\gamma_g^2 + 2J(A_t + A_p + D_p)}}{2J} \approx \sqrt{\frac{A_t + A_p + D_p}{2J}}, \quad (24)$$

where the approximation is valid for $JN_0 \gg \gamma_g$. Therefore, using the equipartition condition obtained from Eq. (21), we obtain

$$\langle n\rangle_{\rm ss} = \langle x^2\rangle_{\rm ss} - \frac{1}{2} \approx \sqrt{\frac{A_t + A_p + D_p}{2J}} - \frac{1}{2}, \quad (25)$$

This result agrees with that in Eq. (14b) of Ref. [1] obtained using the master equation Eq. (1) [the $-1/2$ term was neglected in going from Eq.(14a) to Eq.(14b)]. For higher-order moments, such as $\langle x^4\rangle_{\rm ss}$, required for calculating correlation functions such as $g^{(2)}$, it is difficult to solve the equations of the moments since they involve even higher-order moments. We will calculate those quantities using numerical and analytical solutions to the FP equation in the next section.

III. TRUNCATED WIGNER DISTRIBUTION

In order to study the partial differential equation Eq. (3) in the presence of feedback in more detail, we apply an approximation to the FP equation. This approximation consists of the method of truncated Wigner distributions that has been studied previously [45]. It allows us to keep up to the second-order derivatives in the FP equation, thus retaining both the essential deterministic and stochastic parts.

The justification of the truncation can be understood in two limiting cases. In the first case, when the steady-state phonon number $\langle n\rangle_{\rm ss} \gg 1$, we apply the method of system size expansion to truncate higher-order derivatives [26]. The central idea is that as the system size (measured by the variable $\langle n\rangle_{\rm ss}$ in the present case) increases, the higher-order derivatives can be expanded in terms of a small parameter related to the inverse of the system size. In that case the system variables, x, $p \propto \sqrt{\langle n\rangle_{\rm ss}} \gg 1$, and the higher-order derivatives such as $\partial^4/\partial x^4$ provide much smaller contributions compared to the lower-order derivatives on average.

In the second case, when the steady-state phonon number $\langle n\rangle_{\rm ss} < 1$, we consider the uncertainty principle, i.e. $\Delta x \Delta p \geq 1/2$ to make the truncation. Using this principle for $\langle n\rangle_{\rm ss} < 1$, higher-order derivatives such as $x^2\partial^4/\partial p^4$ and $\partial^6/\partial p^6$ can be shown to be of the same order as $x^4\partial^2/\partial p^2$. In Eq. (3), we therefore retain only the contribution with the coefficient $72\Gamma_f$ from the last term. The truncated FP equation is then given by

$$\frac{\partial W(x,p,t)}{\partial t} = \left(-\omega_z p\frac{\partial}{\partial x} + \omega_z x\frac{\partial}{\partial p}\right) W(x,p,t) + \left[2\gamma_g\frac{\partial}{\partial p}p + (A_t + A_p + D_p)\frac{\partial^2}{\partial p^2} + D_q\frac{\partial^2}{\partial x^2}\right] W(x,p,t) + \left(24\gamma_f x^2\frac{\partial}{\partial p}p + 72\Gamma_f x^4\frac{\partial^2}{\partial p^2}\right) W(x,p,t). \quad (26)$$

Below, we will first recover the results of the master equation analysis of Ref. [1] to show that the truncated FP approach is valid in the range of phonon numbers used in the present article. We will subsequently present new analytical as well as numerical results based on this equation in the low and high damping regimes.

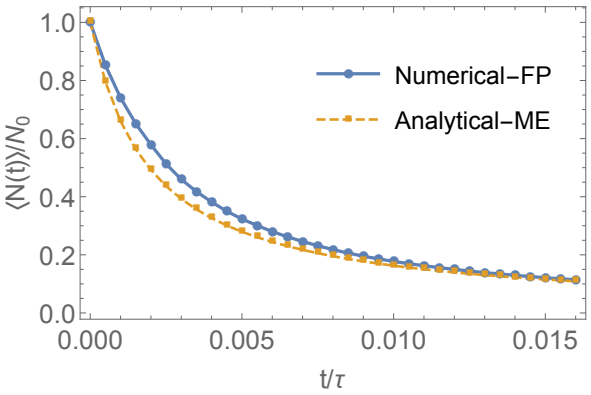

FIG. 2. The scaled phonon number using the numerical simulation of Eq. (26) (solid) and the analytical result in Ref. [1] (dashed) versus time during cooling for initial parameters $\omega_z = 40$ kHz, $\gamma_g = 5$ Hz, $A_t + A_p = 1$ kHz, $\gamma_f = 18\Gamma_f = 2/9$ kHz, and $N_0 = 10^6$. τ is the characteristic time of the nonlinear feedback cooling given in the text.

A. Feedback cooling

In this section we show that our truncated FP approach agrees with earlier results deduced from the master equation [1]. First, we study the dynamical feedback cooling with the FP equation Eq. (26). In Fig. 2, we plot the dynamical phonon number versus t/τ using both the numerical simulation from the FP equation and the analytical result in Ref. [1] obtained with the master equation. Here the characteristic cooling time $\tau = 2\sqrt{(2J + 2\gamma_g)^2 + 8J(A_t + A_p + D_p - J/2)}$. We observe quite good agreement between the two methods.

Next, we study the steady-state phonon number for an initial phonon number $N_0 = 10^6$ for different values of the background gas scattering rate. As shown in Fig. 3, we find good agreement between our numerical results and the earlier analytical result $\langle n\rangle_{\rm ss}$. We observe that

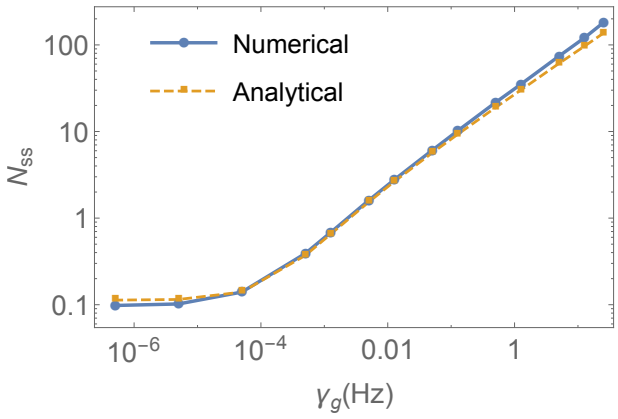

FIG. 3. Steady-state feedback cooling vs background gas damping rate for using the numerical simulation from Eq. (26) (solid) and the analytical expression in Eq. (25) (dashed). The other parameters are the same as in Fig. 2.

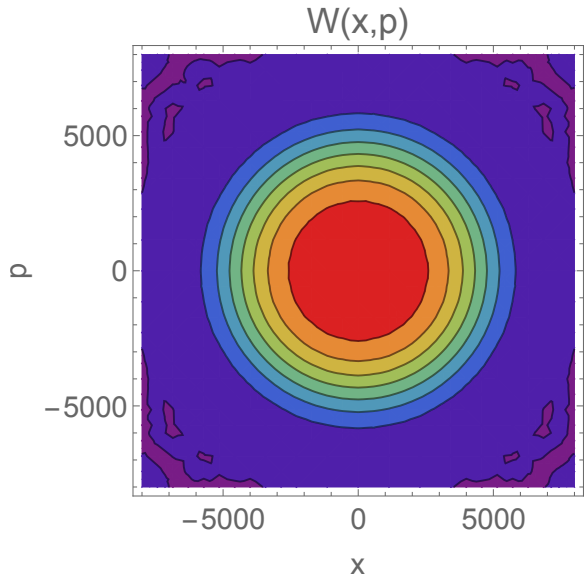

FIG. 4. Steady-state Wigner distribution calculated numerically in the low damping regime for the $\gamma_g = 0.5$ mHz, $A_t + A_p = 1$ kHz, $\gamma_{\rm eff} = 4.45 \times 10^{-7}$ and $N_0 = 10^8$. The steady-state phonon number is $\langle n \rangle_{\rm ns} = 6.68 \times 10^6$.

steady-state phonon number decreases as γ_g is lowered and saturates (i.e. becomes independent of γ_g) for very small γ_g.

The agreement between calculations using the numerical truncated Wigner distribution method [Eq (26)] and the master equation [Eq. (1)] occurs over the entire range of phonon numbers considered in this article and shows the validity of the truncation approximation used by us.

B. Low-damping limit

We now consider the case when both the gas damping rate and the parametric feedback damping rate are much smaller than the mechanical oscillation frequency. From Eq. (26), it can be seen that this limit corresponds to the condition

$$\frac{2\gamma_g + 24\gamma_f \langle x^2 \rangle_{\rm ss}}{\omega_z} \approx \gamma_{\rm eff} \ll 1, \tag{27}$$

where we have considered the low-gas-pressure limit in the second step, and

$$\gamma_{\rm eff} = \frac{24\gamma_f \langle x^2 \rangle_{\rm ss}}{\omega_z}. \tag{28}$$

Solving Eq. (26) numerically in this regime, we obtain the Wigner function shown in Fig. 4. We observe only a single peak in the Wigner distribution well localized near the origin due to the parametric feedback.

To analyze the phase-space distribution further, we define the dimensionless energy of the system as $\epsilon = (x^2 + p^2)/2$, where $x = \sqrt{2\epsilon}\cos(\omega_z t)$ and $p = \sqrt{2\epsilon}\sin(\omega_z t)$. Since we have assumed the harmonic oscillation frequency of the nanoparticle to be much higher than the damping rate, averaging on the timescale of $1/\omega_z$, yields $x^2 \approx p^2 \approx \epsilon$. For $\langle x^2 \rangle_{\rm ss} \gg 1$, the low feedback damping implied by Eq. (27) corresponds to small feedback gain, i. e., $G \ll 1$, and we can neglect the feedback backaction term in Eq. (26). With these conditions, we can write the truncated FP equation in phase-space in terms of the energy variable as

$$\begin{aligned}&\frac{\partial W_\epsilon(\epsilon,t)}{\partial t} \\ &\approx \frac{\partial}{\partial \epsilon}\left[2\gamma_g\left(\epsilon - \frac{A_t + A_p + D_p}{2\gamma_g}\right) + 12\gamma_f\epsilon^2\right] W_\epsilon(\epsilon,t) \\ &+(A_t + A_p + D_p)\frac{\partial^2}{\partial \epsilon^2}\epsilon W_\epsilon(\epsilon,t),\end{aligned} \tag{29}$$

where we have dropped both the feedback backaction and the position diffusion terms, and also assume $x^2p^2 \approx \epsilon^2/2$ when averaged over a period of mechanical oscillation. We were able to solve Eq. (29) analytically in the steady state for the energy distribution

$$W_{\epsilon \rm ss}(\epsilon) = \mathcal{N} \exp\left[-\frac{2\gamma_g}{A_t + A_p + D_p}\left(\epsilon + \frac{3\gamma_f}{\gamma_g}\epsilon^2\right)\right] \tag{30}$$

where $\mathcal{N}$ is a normalization constant. The FP equation [Eq. (29)] and its steady state solution [Eq. (30)] for the energy are exactly the same as obtained earlier using a classical analysis and verified experimentally [2, 10]. The origin of the deviation from a Boltzmann distribution can be seen clearly to be the nonlinear parametric feedback cooling in Eq. (30). The steady state phonon number can be calculated analytically from Eq. (30) as $\langle n \rangle = \int \epsilon W_{\epsilon \rm ss}(\epsilon) d\epsilon$, but the expression is rather cumbersome and we do not reproduce it here. Calculating the mean phonon number using both the analytical expression derived from Eq. (30) and the numerical simu-

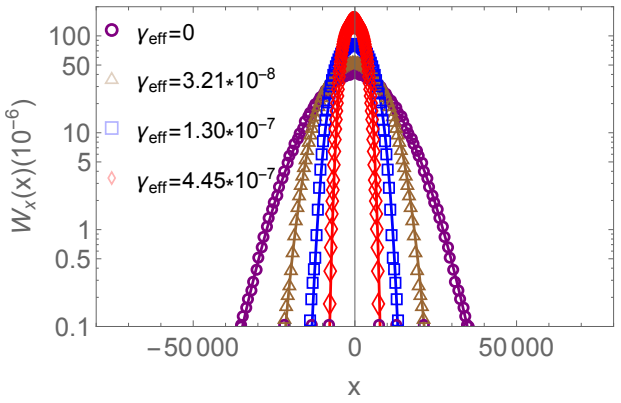

FIG. 5. Position distributions for different feedback strengths $\gamma_{\rm eff}$ using both the analytical expression (solid lines)[Eq. (31)] and the numerical simulation (dotted symbols). The remaining parameters are the same as in Fig. 4.

lation for the parameters of Fig. 4, gives the same result, $\langle n_{\rm ns}\rangle = 6.68\times10^6$.

By replacing $\epsilon = (x^2+p^2)/2$ and performing an integration on the momentum p in Eq. (30), we obtain an analytical expression for the position distribution in this low-damping limit,

$$W_{\rm ess}(x) = \mathcal{N}'\sqrt{3x^2\gamma_f+\gamma_g}\exp\left[-\frac{(3x^2\gamma_f+\gamma_g)^2}{12\gamma_f(A_t+A_p+D_p)}\right] \times K_{\frac{1}{4}}\left[\frac{(3x^2\gamma_f+\gamma_g)^2}{12\gamma_f(A_t+A_p+D_p)}\right], \quad (31)$$

where $\mathcal{N}'$ is a normalization constant and $K_{\frac{1}{4}}$ is a generalized Bessel function of the second kind. This expression for the position distribution agrees with that derived classically in Ref. [2, 10], in the absence of driving, nonlinearity and feedback backaction. We plot the position distribution using both the analytical expression of Eq. (31) and the full numerical simulation of Eq. (26) in Fig. 5. As can be seen, both methods agree well with each other, and also with Fig.1 in Ref. [10].

To conclude, in this section we demonstrated that in the low damping limit, our quantum calculations show agreement with earlier classical calculations, which now provides us with a tool for examining the quantum-to-classical transition. This agreement also demonstrates that our truncation of the FP equation is valid in the low-damping limit.

C. Overdamped limit

We now consider the regime in which the nanoparticle motion is overdamped. The numerical solution of Eq. (26) yields a double-peaked Wigner function as shown in Fig. 6. This behavior is unlike that in the low-damping regime, as can be seen readily by comparing Figs. 4 and 6. It is also distinct from earlier bimodal distributions which were observed in the presence of external driving of the nanoparticle [2]; in our case, there is no such driving.

In order to investigate further, we consider analytical solutions to Eq. (26). However, even with the truncation of higher-order derivatives in the Wigner distribution, the FP equation [Eq. (26)] is difficult to solve analytically because of the presence of the nonlinear feedback. We find it is more convenient to first consider the corresponding quantum Langevin equations for the nanoparticle derived from Eq. (3) the full FP equation [43]

$$\dot{x} = \omega_z p + F_x(t), \quad (32)$$
$$\dot{p} = -\omega_z x - 2\gamma_g p - 24\gamma_f x^2 p + F_p(t), \quad (33)$$

where the correlations of the noises are given explicitly as

$$\langle F_x(t)F_x(t')\rangle = 2D_q\delta(t-t'), \quad (34)$$
$$\langle F_p(t)F_p(t')\rangle = \left[2(A_t+A_p+D_p)+144\Gamma_f x^4\right]\delta(t-t'). \quad (35)$$

In the overdamped regime, the condition

$$\frac{2\gamma_g+24\gamma_f\langle x^2\rangle_{\rm ss}}{\omega_z} \approx \gamma_{\rm eff} \gtrsim 1, \quad (36)$$

applies. Here we consider the gas damping rate $\gamma_g \ll \omega_z$, which does not contribute significantly to strong damping [46]. For experimentally accessible parameters [1], $\gamma_f \ll \omega_z$ which gives $\langle x^2\rangle_{\rm ss} \gg 1$ as the condition for overdamping. We consider the situation $(2\gamma_g+24\gamma_f x^2)p \gg \dot{p}$ in Eq. (33), which implies $\dot{p}\approx 0$, and allows us to eliminate the momentum adiabatically. We then obtain from Eq. (33) $p \approx -(\omega_z x - F_p(t))/(2\gamma_g+24\gamma_f x^2)$. Substituting into Eq. (32), the quantum Langevin equation for the nanoparticle's position can be approximated as

$$\dot{x} \approx -\frac{\omega_z^2 x}{2\gamma_g+24\gamma_f x^2} + \frac{\omega_z F_p(t)}{2\gamma_g+24\gamma_f x^2}, = h(x,t)+g(x,t)\Gamma(t), \quad (37)$$

where we have dropped the position fluctuation force $F_x(t)$, which is negligible because $D_q \ll \omega_z$ and define

$$h(x,t) = -\frac{\omega_z^2 x}{2\gamma_g+24\gamma_f x^2}, \quad (38)$$
$$g(x,t) = \frac{\omega_z\sqrt{A_t+A_p+D_p+72\Gamma_f x^4}}{2\gamma_g+24\gamma_f x^2}, \quad (39)$$

and $\langle\Gamma(t)\Gamma(t')\rangle = 2\delta(t-t')$.

1. *The position distribution*

According to Ref. [43], the FP equation for the position of the nanoparticle corresponding to Eq. (37) is given by

$$\frac{\partial W_x(x,t)}{\partial t} = -\frac{\partial}{\partial x}\left(D_x^{(1)}W_x(x,t)\right) + \frac{\partial^2}{\partial x^2}\left(D_x^{(2)}W_x(x,t)\right), \quad (40)$$

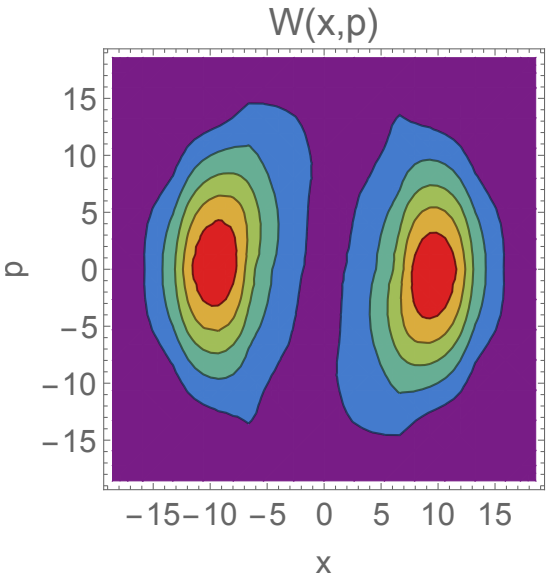

FIG. 6. Steady-state Wigner distribution obtained numerically in the high feedback damping regime for $\gamma_g = 0.05$ Hz, $\gamma_f = 27\Gamma_f = 4/27$ kHz, and $N_0 = 10^8$. The other parameters are the same as in Fig. 2. The steady-state phonon number is $\langle n \rangle_{\rm ns} \approx 84$.

where $D_x^{(1)} = h(x,t) + \frac{\partial g(x,t)}{\partial x} g(x,t)$, $D_x^{(2)} = (g(x,t))^2$, and $W_x(x,t) = \int W(x,p,t)dp$. In the steady-state, Eq. (40) can be solved analytically to yield the position distribution

$$W_{x\rm ss}(x) = \mathcal{N}_x \frac{\gamma_g + 12x^2\gamma_f}{(A_t + A_p + D_p + 72\Gamma_f x^4)^{\frac{\gamma_f + 6\Gamma_f}{12\Gamma_f}}} \times \exp\left[-\frac{\gamma_g \arctan\left(6\sqrt{2}x^2 \sqrt{\frac{\Gamma_f}{A_t + A_p + D_p}}\right)}{6\sqrt{2\Gamma_f (A_t + A_p + D_p)}} \right], \quad (41)$$

where $\mathcal{N}_x$ is a normalization constant.

In Fig. 7, we have plotted the analytical expression for $W_{x\rm ss}(x)$ from Eq. (41) as well as the numerical solution from Eq. (26). Both results show two peaks, which is indicative of bistability. To investigate further, we consider the condition $\gamma_g \ll \sqrt{\Gamma_f (A_t + A_p + D_p)}$ for which the exponential term in Eq. (41) can be dropped as it is almost unity for the range of the position distribution. This condition is equivalent to $N_0 \Gamma_f \gg \gamma_g$ which is valid for the parameter regime we study here. Then the position distribution reduces to

$$W_{x\rm ss}(x) \simeq \frac{12\mathcal{N}_x \gamma_f x^2}{(A_t + A_p + D_p + 72\Gamma_f x^4)^{\frac{\gamma_f + 6\Gamma_f}{12\Gamma_f}}}. \quad (42)$$

From this expression we see that the term $\propto \gamma_f x^2$ in the numerator, which corresponds to feedback cooling, pushes the particle away from the origin $x = 0$, by making the position distribution vanish at that point. This

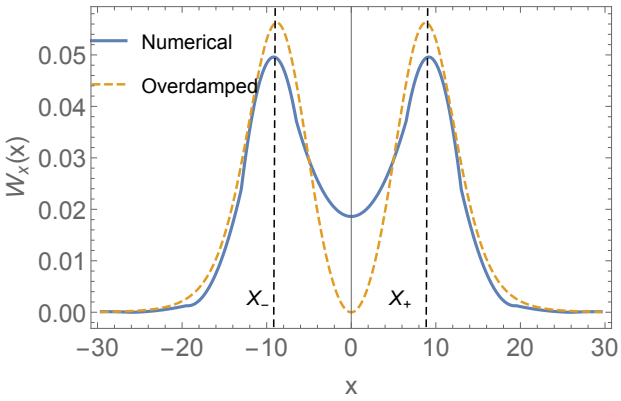

FIG. 7. Steady-state position distributions from the numerical solution (solid) of Eq. (26) and that using $W_{x\rm ss}(x)$ [Eq. (41)] (dashed) for the same parameters in Fig. 6.

can be understood intuitively from the fact that the feedback force is $\propto -x^2 p$ [13], which vanishes at the origin and allows the particle to transit that point without slowing down. In contrast, the term $\propto \Gamma_f x^4$ in the denominator of Eq. (42), which is due to feedback backaction noise, pushes the particle towards the origin, by making the position distribution there large. We may therefore expect equilibria away from the origin. These can be found by taking the derivative of Eq. (42) with respect to x, and we obtain two maxima corresponding to

$$x_\pm = \pm \left(\frac{A_t + A_p + D_p}{2J} \right)^{\frac{1}{4}} = \pm \sqrt{\langle x^2 \rangle_{\rm ss}}, \quad (43)$$

i.e. the equilibria correspond to the mean values found in Eq. (24). To corroborate, we calculate the mean values implied by Eq. (42),

$$\langle x^2 \rangle_{W\rm ss} = \sqrt{\frac{A_t + A_p + D_p}{72\Gamma_f}} \frac{\Gamma\left[\frac{5}{4}\right] \Gamma\left[\frac{\gamma_f}{12\Gamma_f} - \frac{3}{4}\right]}{\Gamma\left[\frac{3}{4}\right] \Gamma\left[\frac{\gamma_f}{12\Gamma_f} - \frac{1}{4}\right]}, \quad (44)$$

where $\Gamma[m]$ is the Gamma function with a variable m. At optimum feedback [1], $\gamma_f = 18\Gamma_f$, we find $\langle x^2 \rangle_{W\rm ss} = \sqrt{3}\sqrt{\frac{A_t + A_p + D_p}{2J}}$ which is $\sqrt{3}$ times larger than the quantity calculated in Eq. (24) using the full FP equation. The explanation for this difference derives from the assumption of overdamped motion, which significantly reduces the probability of finding the nanoparticle around $x = 0$. With this assumption therefore, the moment of $\langle x^2 \rangle_{W\rm ss}$ is greater than the quantity calculated without the overdamped approximation. The analytical result of $x_\pm$ [Eq. (43)] agrees quite well with the locations of the peaks of the position distribution as can be seen from the dashed vertical lines in Fig. 7.

In order to understand the bistability from the perspective of energy, we consider the non-equilibrium nanoparticle potential [37]

$$U(x) = -k_B T \ln[W_{x\rm ss}(x)], \quad (45)$$

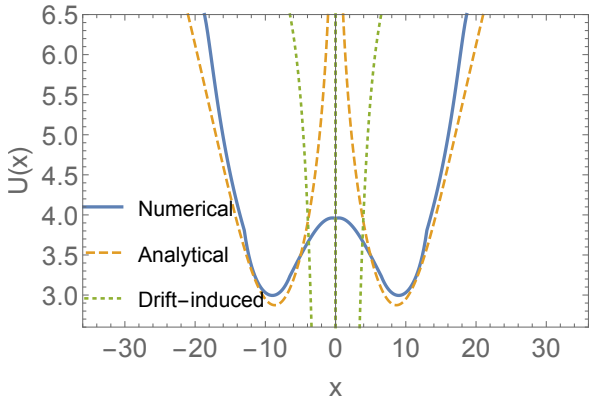

FIG. 8. The non-equilibrium nanoparticle potential $U(x)$ [Eq. (45)] as a function of scaled nanoparticle displacement x/x_0. The solid curve is the result of numerically solving Eq. (26), the dashed curve corresponds to the analytical result found using Eq. (41), and the dotted curve is drift-induced potential obtained using $h(x,t)$ from Eq. (37) for the same parameters in Fig. 6

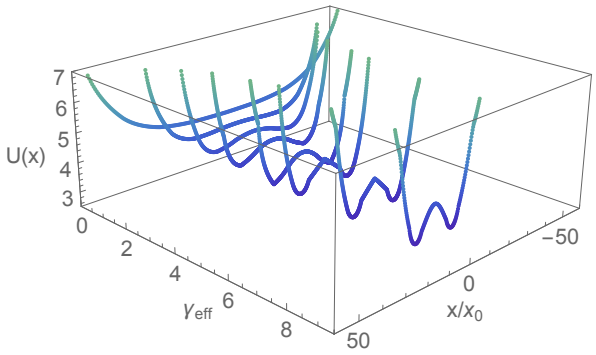

FIG. 9. Full non-equilibrium nanoparticle potential as a function of feedback strength $\gamma_{\rm eff}$. As the feedback increases, the potential changes from simple harmonic to bistable. The other parameters are the same as in Fig. 6.

where $\ln[x]$ is the natural logarithm of x. We show the analytical potential found by combining Eq. (45) and Eq. (41) as well as the corresponding numerical calculation from Eq. (26) in Fig. 8. Both curves show that the potential $U(x)$ exhibits double minima that correspond to nanoparticle bistability. The analytical curve overestimates the barrier between the two wells due to the assumption of overdamping. The numerical curve presents a lower barrier.

We emphasize that in contrast to cavity optomechanics [20, 32–34, 39], bistability in our model cannot be explained by solely considering the mean effects of the feedback and neglecting the fluctuating terms in the Langevin equation. This can be seen by plotting the potential of Eq. (45) obtained by setting $g(x,t) = 0$. This potential, which is entirely due to the nonfluctuating contribution $h(x,t)$ in the Langevin equation of Eq. (37), is shown as a dotted curve in Fig. 8 and clearly does not exhibit the shape required to explain bistability. For the parameters used to calculate the full potential which includes the stochastic processes of the system, we find the gas fluctuations represented by D_p form the dominant diffusive contribution to the bistability, while the effects of optical scattering and feedback backaction are small.

In order to show how the bistability turns on, we have also plotted in Fig. 9 the evolution of the non-equilibrium nanoparticle potential $U(x)$, obtained by solving Eq. (26), as a function of the feedback cooling strength $\gamma_{\rm eff}$. As can be seen, with increasing feedback, the potential changes from simple harmonic to bistable. The corresponding plot for the maxima of the nanoparticle position distribution as a function of $\gamma_{\rm eff}$ is shown in Fig. 10. It should be noted while considering these plots that the maximum allowed value of the feedback strength is restricted by the modulation of the trap laser beam intensity [1],

$$M = \frac{\gamma_f \langle n \rangle_{\rm ss}}{\omega_z}, \tag{46}$$

which cannot be more than 100%. As we can see from Fig. 10, the bistability already starts to appear at $M \approx 5\%$. We note for very high modulation values, it may be necessary to include higher-order sidebands to increase the accuracy of the calculation. Also we note here that we presented feedback-induced bistability for low steady-state phonon numbers ($\langle n \rangle_{\rm ss} < 100$). However, bistability may be obtained even for high phonon numbers as long as the condition Eq. (36) is satisfied. For example, we have verified the presence of bistability for $\gamma_g = 0.5$ kHz, $\gamma_f = 3.3 \times 10^{-5}$ kHz, $\Gamma_f = 2.8 \times 10^{-10}$ kHz, which imply $\gamma_{\rm eff} = 9.9$ and $\langle n \rangle_{\rm ss} = 3.53 \times 10^5$, conditions that may be easier to realize experimentally. To be concrete, these parameters correspond to an experimental setup of a fused silica nanoparticle 50 nm in radius levitated by a 1064 nm trap (100 mW) and probed by a separate beam (10 mW) in a vacuum of 1 mbar at room temperature [1, 16].

We conclude this section by stating one advantage of the FP approach, which is that any moment can be calculated directly by performing integration using the Wigner function. This is important especially for finding higher-order moments which are difficult to obtain directly using the master equation Eq. (1), as pointed out in Section II B. For example, for optimum feedback, we obtain the fourth order steady-state moment by integration

$$\langle x^4 \rangle_{W\rm ss} = \frac{9(A_t + A_p + D_p)}{2J} = 3 \langle x^2 \rangle^2_{W\rm ss}, \tag{47}$$

which is the same as that for a zero-mean Gaussian distribution and was assumed for the position distribution in Section II B.

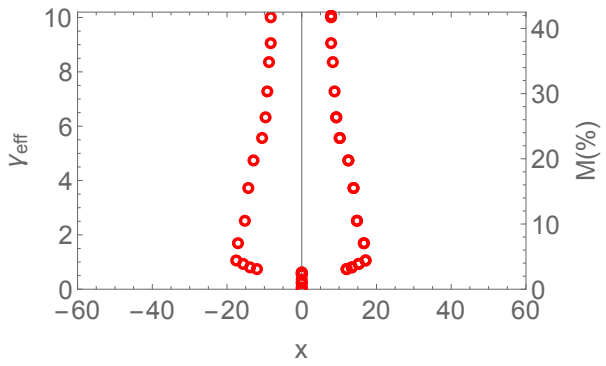

FIG. 10. The maxima in the nanoparticle position distributions as a function of feedback strength $\gamma_{\rm eff}$. As the feedback increases, the monostable solution turns into a bistable solution. The modulation of the trap laser beam intensity is also indicated on the right vertical axis. The other parameters are the same as in Fig. 6.

2. *The momentum distribution*

We now consider the momentum distribution in the overdamped regime. Interestingly, it turns out to be analytically more accessible than the position distribution, thus making the calculation of higher moments more amenable. By performing an integration on x on both sides of Eq. (26), we obtain the following FP equation for the momentum distribution

$$\frac{\partial W_p(p,t)}{\partial t} = -\frac{\partial}{\partial p}\left(D_p^{(1)} W_p(p,t)\right) + \frac{\partial^2}{\partial p^2}\left(D_p^{(2)} W_p(p,t)\right), \tag{48}$$

where $D_p^{(1)} = -2\gamma_g p - 24\gamma_f \langle x^2\rangle_{W\rm ss} p$ and $D_p^{(2)} = (A_t + A_p + D_p) + 72\Gamma_f \langle x^4\rangle_{W\rm ss}$. In the steady-state, the momentum distribution can be obtained analytically in the form of a Gaussian function given by

$$W_{p\rm ss}(p) = \mathcal{N}_p \exp\left(-\frac{\gamma_g + 12\gamma_f \langle x^2\rangle_{W\rm ss}}{(A_t + A_p + D_p) + 72\Gamma_f \langle x^4\rangle_{W\rm ss}} p^2\right), \tag{49}$$

where $\mathcal{N}_p$ is a normalization constant. The momentum distribution of Eq. (49) as well as the corresponding quantity calculated from Eq. (26) are shown in Fig. 11, and agree quite well with each other. We obtain from Eq. (49) the second and fourth order moments as

$$\begin{aligned}\langle p^2\rangle_{W\rm ss} &= \frac{(A_t + A_p + D_p) + 72\Gamma_f \langle x^4\rangle_{W\rm ss}}{2\gamma_g + 24\gamma_f \langle x^2\rangle_{W\rm ss}} \\ &= \sqrt{\frac{A_t + A_p + D_p}{3J/2}},\end{aligned} \tag{50}$$

$$\langle p^4\rangle_{W\rm ss} = 3\langle p^2\rangle_{W\rm ss}^2 = 2\left(\frac{A_t + A_p + D_p}{J}\right). \tag{51}$$

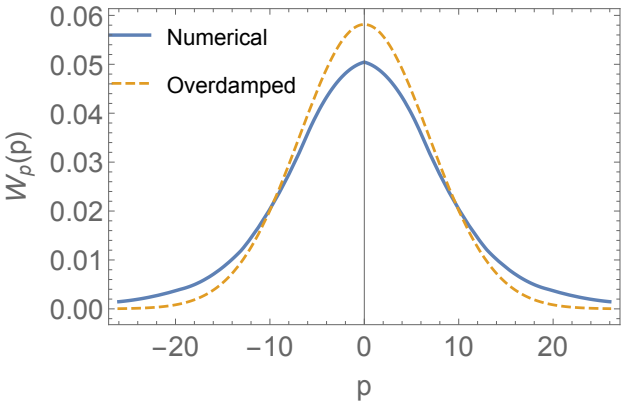

FIG. 11. Steady-state momentum distributions from the numerical solution (solid) and that using $W_{p\rm ss}(p)$ (dashed) for the same parameters in Fig. 6.

From these expressions, we obtain the steady-state mean phonon number

$$\langle n\rangle_{W\rm ss} = \frac{5}{2\sqrt{3}}\sqrt{\frac{A_t + A_p + D_p}{2J}} - \frac{1}{2}, \tag{52}$$

which qualitatively agrees with the result of Eq. (24). For the parameters of Fig. 6, we calculate the mean phonon number $\langle n\rangle_{\rm ns} = 84$ using the numerical solution to Eq. (26). This result is close to the analytical results $\langle n\rangle_{\rm ss} = 65$ [Eq. (25)] and $\langle n\rangle_{\rm Wss} = 75$ [Eq. (52)]. The mean of the phonon number squared is given by

$$\begin{aligned}\langle n^2\rangle_{W\rm ss} &= \int W_{\rm ss}(x,p)\left[\left(\frac{x^2+p^2}{2}\right)^2 - \left(\frac{x^2+p^2}{2}\right)\right] dxdp \\ &\approx \frac{1}{4}\left(\langle x^4\rangle_{W\rm ss} + 2\langle x^2\rangle_{W\rm ss}\langle p^2\rangle_{W\rm ss} + \langle p^4\rangle_{W\rm ss}\right) \\ &\quad -\frac{1}{2}\left(\langle x^2\rangle_{W\rm ss} + \langle p^2\rangle_{W\rm ss}\right) \\ &= \frac{17}{8}\frac{A_t + A_p + D_p}{J} - \frac{5}{2\sqrt{3}}\sqrt{\frac{A_t + A_p + D_p}{2J}}.\end{aligned} \tag{53}$$

Therefore, the second-order correlation function for the feedback-cooled nanoparticle in the overdamped regime is given by

$$\begin{aligned}g^{(2)} &= \frac{\langle n^2\rangle_{W\rm ss} - \langle n\rangle_{W\rm ss}}{\langle n\rangle_{W\rm ss}^2} \\ &\approx \frac{51}{25},\end{aligned} \tag{54}$$

where we consider the overdamped condition $\langle x^2\rangle_{W\rm ss} \gg 1$ to obtain the last line. This result shows that in the overdamped regime the nanoparticle has a phonon bunching relation close to a thermal mechanical state for which $g^{(2)} = 2$ [1].

IV. CONCLUSION

In conclusion, we have studied the low and high damping regimes for an optically levitated nanoparticle subject to parametric feedback. We have used a Fokker Planck treatment, useful for viewing the phase-space distribution of the nanoparticle and calculating higher-order moments of the oscillator variables in the presence of nonlinear feedback. For low damping, we obtained the position and energy distributions of Ref. [2, 10], but starting from a fully quantum mechanical model. For high damping, we found a feedback-induced bistability. It is important to note that unlike in the case of cavity-based systems, the bistability manifests itself only in the mechanical, and not optical, degree of freedom. Also, the bistability is crucially influenced by system fluctuations and therefore cannot be described using a classical mean value equation as in standard cavity optomechanics. Our prediction should be experimentally observable as we have used realistic parameters in our analysis. Using our formalism we have also investigated energy equipartition, phonon number behavior, and phonon bunching for the nanoparticle, which shows close resemblance to that of a thermal mechanical state. We presented both analytical and numerical results to support our conclusions. Our study opens the door to the use of bistability in cavity-free levitated systems, and provides a framework for studying the phase-space properties of such systems.

ACKNOWLEDGMENTS

This research is supported by the Office of Naval Research under Award No. N00014-14-1-0803. We thank A. N. Vamivakas, J. Sipe, B. Zwickl, R. Pettit, L. Neukirch, and C. Zou for useful discussions.

[1] B. Rodenburg, L. P. Neukirch, A. N. Vamivakas, and M. Bhattacharya, "Quantum model of cooling and force sensing with an optically trapped nanoparticle," Optica **3**, 318–323 (2016).

[2] J. Gieseler, R. Quidant, C. Dellago, and L. Novotny, "Dynamic relaxation of a levitated nanoparticle from a non-equilibrium steady state," Nat. Nano. **9**, 358 (2014).

[3] A. Ashkin, "Acceleration and trapping of particles by radiation pressure," Phys. Rev. Lett. **24**, 156–159 (1970).

[4] S. Chu, J. E. Bjorkholm, A. Ashkin, and A. Cable, "Experimental observation of optically trapped atoms," Phys. Rev. Lett. **57**, 314–317 (1986).

[5] A. Ashkin, J. M. Dziedzic, J. E. Bjorkholm, and S. Chu, "Observation of a single-beam gradient force optical trap for dielectric particles," Opt. Lett. **11**, 288–290 (1986).

[6] A. Ashkin and J. Dziedzic, "Optical trapping and manipulation of viruses and bacteria," Science **235**, 1517–1520 (1987).

[7] T. Li, S. Kheifets, and M. G. Raizen, "Millikelvin cooling of an optically trapped microsphere in vacuum," Nat. Phys. **7**, 527(2011).

[8] Z. Q. Yin, A. A. Geraci, and T. Li,"Optomechanics of levitated dielectric particles," International Journal of Modern Physics B **27**, 1330018(2013).

[9] Y. Arita, M. Mazilu, and K. Dholakia, "Laser-induced rotation and cooling of a trapped microgyroscope in vacuum," Nat. Commun. **4**, 2374 (2013).

[10] J. Gieseler, L. Novotny, C. Moritz, and C. Dellago, "Non-equilibrium steady state of a driven levitated particle with feedback cooling," New Journal of Physics **17**, 045011 (2015).

[11] J. Millen, T. Deesuwan, P. Barker, and J. Anders, "Nanoscale temperature measurements using non-equilibrium Brownian dynamics of a levitated nanosphere," Nat. Nano. **9**, 425–429 (2014).

[12] J. Gieseler, M. Spasenović, L. Novotny, and R. Quidant, "Nonlinear mode coupling and synchronization of a vacuum-trapped nanoparticle," Phys. Rev. Lett. **112**, 103603 (2014).

[13] L. P. Neukirch and A. N. Vamivakas, "Nano-optomechanics with optically levitated nanoparticles," Contemporary Physics **56**, 48–62 (2015).

[14] D. E. Chang, C. A. Regal, S. B. Papp, D. J. Wilson, J. Ye, O. Painter, H. J. Kimble, and P. Zoller, "Cavity opto-mechanics using an optically levitated nanosphere," Proc. Natl. Acad. Sci. USA **107**, 1005 (2010).

[15] N. Kiesel, F. Blaser, U. Delić, D. Grass, R. Kaltenbaek, and M. Aspelmeyer, "Cavity cooling of an optically levitated submicron particle," Proceedings of the National Academy of Sciences **110**, 14180–14185 (2013).

[16] J. Gieseler, B. Deutsch, R. Quidant, and L. Novotny, "Subkelvin parametric feedback cooling of a laser-trapped nanoparticle," Phys. Rev. Lett. **109**, 103603 (2012).

[17] O. Romero-Isart, A. C. Pflanzer, F. Blaser, R. Kaltenbaek, N. Kiesel, M. Aspelmeyer, and J. I. Cirac, "Large quantum superpositions and interference of massive nanometer-sized objects," Phys. Rev. Lett. **107**, 020405 (2011).

[18] P. Meystre, "A short walk through quantum optomechanics," Annalen der Physik **525**, 215–233 (2013).

[19] Y. Chen, "Macroscopic quantum mechanics: theory and experimental concepts of optomechanics," Journal of Physics B: Atomic, Molecular and Optical Physics **46**, 104001 (2013).

[20] M. Aspelmeyer, T. J. Kippenberg, and F. Marquardt,"Cavity optomechanics," Rev. Mod. Phys. **86**, 1391–1452 (2014).

[21] J. Q. Liao and L. Tian, "Macroscopic quantum superposition in cavity optomechanics", Phys. Rev. Lett. **116**, 163602 (2016).

[22] A. A. Geraci, S. B. Papp, and J. Kitching, "Short-range force detection using optically cooled levitated microspheres," Phys. Rev. Lett. **105**, 101101 (2010).

[23] A. Arvanitaki and A. A. Geraci, "Detecting high-frequency gravitational waves with optically levitated

sensors," Phys. Rev. Lett. **110**, 071105 (2013).
[24] D. C. Moore, A. D. Rider, and G. Gratta, "Search for millicharged particles using optically levitated microspheres," Phys. Rev. Lett. **113**, 251801 (2014).
[25] G. Ranjit, D. P. Atherton, J. H. Stutz, M. Cunningham,and A. A.Geraci, "Attonewton force detection using microspheres in a dual-beam optical trap in high vacuum," Phys. Rev. A **91**, 051805 (2015).
[26] H. J. Carmichael, *Statistical Methods in Quantum Optics 1: Master Equations and Fokker-Planck Equations* (Springer, 2002).
[27] S. Mancini, D. Vitali, and P. Tombesi, "Optomechanical cooling of a macroscopic oscillator by homodyne feedback," Phys. Rev. Lett. **80**, 688 (1998).
[28] D. J. Wilson, V. Sudhir, N. Piro, R. Schilling, A. Ghadimi, and T. J. Kippenberg, "Measurement-based control of a mechanical oscillator at its thermal decoherence rate", Nature **524**, 325(2015).
[29] A. G. Krause, T. D. Blasius, and O. Painter, "Optical read out and feedback cooling of a nanostring optomechanical cavity", arXiv:1506.01249 (2015).
[30] V. Sudhir, D. J. Wilson, R. Schilling, H. Schütz, A. Ghadimi, A. Nunnenkamp, and T. J. Kippenberg. "Appearance and disappearance of quantum correlations in measurement-based feedback control of a mechanical oscillator." arXiv:1602.05942 (2016).
[31] C. Genes, D. Vitali, P. Tombesi, S. Gigan, and M. Aspelmeyer, "Ground-state cooling of a micromechanical oscillator: Comparing cold damping and cavity-assisted cooling schemes", Phys. Rev. A **77**, 033804(2008).
[32] A. Dorsel, J. D. McCullen, P. Meystre, E. Vignes, and H. Walther, "Optical bistability and mirror confinement induced by radiation pressure", Phys. Rev. Lett., **51**, 1550 (1983).
[33] P. Meystre, E. M. Wright, J. D. McCullen, and E. Vignes, "Theory of radiation-pressure-driven interferometers", J.O.S.A. B, **2**, 1830 (1985).
[34] C. Metzger, M. Ludwig, C. Neuenhahn, A. Ortlieb, I. Favero, K. Karrai, and F. Marquardt, "Self-induced oscillations in an optomechanical system driven by bolometric backaction", Phys. Rev. Lett., **101**, 133903(2008).
[35] F. Mueller, S. Heugel, and L. J. Wang, "Observation of optomechanical multistability in a high-Q torsion balance oscillator", Phys. Rev. A, **77**, 031802(R)(2008).
[36] H. Xu, U. Kemiktarak, J. Fan, S. Ragole, J. Lawall, and J. M. Taylor, "Observation of optomechanical buckling phase transistions", arxiv:1510.04971 (2015)
[37] M. Kus, K. Wodkiewicz, and J. A. C. Gallas, "Absorptive optical bistability with laser-amplitude fluctuations", Phys. Rev. A, **28**, 314 (1983).
[38] C. Genes, A. Mari, P. Tombesi, and D. Vitali, "Robust entanglement of a micromechanical resonator with output optical fields", Phys. Rev. A **78**, 032316 (2008).
[39] R. Ghobadi, A. R. Bahrampour and C. Simon, "Quantum optomechanics in the bistable regime", Phys. Rev. A **84**, 033846 (2011).
[40] F. Marquardt, J. G. E. Harris, and S. M. Girvin, "Dynamical multistability induced by radiation pressure in high-finesse micromechanical optical cavities", Phys. Rev. Lett. **96**, 103901 (2006).
[41] L.Diósi "Quantum master equation of a particle in a gas environment," EPL (Europhysics Letters) **30**, 63 (1995).
[42] M. O. Scully and M. S. Zubairy, *Quantum Optics* (Cambridge University Press, New York, 1997).
[43] H. Risken, *The Fokker-Planck Equation: Methods of Solution and Applications* (Springer, 1984).
[44] There are eight independent boundary conditions for the partial differential equation (3), which is second-order in x and sixth-order in p. They are $\frac{\partial^j W(x,p,t)}{\partial^j x}|_{x=+\infty} = 0$ $(j = 0, 1)$, and $\frac{\partial^k W(x,p,t)}{\partial p^k}|_{p=+\infty} = 0$ $(k = 0, 1, 2, 3, 4, 5)$. By observing from Eq. (3), we find $W(x, p, t) = W(-x, -p, t)$, which implies $\frac{\partial^j W(x,p,t)}{\partial^j x}|_{x=-\infty} = 0$ $(j = 0, 1)$, and $\frac{\partial^k W(x,p,t)}{\partial p^k}|_{p=-\infty} = 0$ $(k = 0, 1, 2, 3, 4, 5)$.
[45] M. Werner and P. Drummond, "Robust algorithms for solving stochastic partial differential equations," Journal of Computational Physics **132**, 312–326 (1997).
[46] F. Haake and R. Reibold, "Strong damping and low-temperature anomalies for the harmonic oscillator", Phys. Rev. A **32**, 2462 (1985).